Top-quark mass effects in $H+$jet and $H+2$ jets production

X. Chen,[a,b,c] A. Huss,[d] S.P. Jones,[e] M. Kerner,[a,b,c] J.-N. Lang,[c] J.M. Lindert[f] and H. Zhang[c,g]

[a] *Institute for Theoretical Physics, Karlsruhe Institute of Technology,*
76131 Karlsruhe, Germany

[b] *Institute for Astroparticle Physics, Karlsruhe Institute of Technology,*
76344 Eggenstein-Leopoldshafen, Germany

[c] *Physik-Institut, Universität Zürich,*
CH-8057 Zürich, Switzerland

[d] *Theoretical Physics Department, CERN,*
1211 Geneva 23, Switzerland

[e] *Institute for Particle Physics Phenomenology, Durham University,*
Durham, DH1 3LE, U.K.

[f] *Department of Physics and Astronomy, University of Sussex,*
Brighton BN1 9QH, U.K.

[g] *Institut für Theoretische Teilchenphysik, Karlsruhe Institute of Technology,*
76128 Karlsruhe, Germany

E-mail: xuan.chen@kit.edu, alexander.huss@cern.ch,
stephen.jones@durham.ac.uk, matthias.kerner@kit.edu,
jlang@physik.uzh.ch, j.lindert@sussex.ac.uk, hantian.zhang@kit.edu

ABSTRACT: We present calculations of Higgs boson production via gluon-gluon fusion in association with one or two additional jets at next-to-leading order in QCD. The calculation of $H+$jet is exact in the treatment of the top-quark mass, whereas for the $H+2$ jets calculation the two-loop virtual amplitudes are approximated via a reweighting with leading-order mass effects, while keeping all top-quark mass effects in the real radiation contributions. For $H+$jet production, this study extends a previous calculation, revealing an error in the previous results. For total and differential cross sections, we present new results and compare the QCD corrections with the infinite top-mass limit, for which we find a strikingly good agreement if all amplitudes are rescaled by the leading-order mass dependence.

Contents

1 Introduction

The current and upcoming runs of the Large Hadron Collider (LHC) are stress-testing the Standard Model (SM) of particle physics at an unprecedented level. In this respect one of the main objectives of Run 3 and the high-luminosity phase of the LHC (HL-LHC) will be a further detailed investigation of the Higgs sector. The abundant future data samples will allow the range of Higgs analyses to be extended to multi-dimensional measurements and high-energy tails of kinematic distributions. A key observable in this regard is the transverse momentum distribution of the Higgs boson, $p_{\mathrm{T,H}}$, which serves as a unique probe of physics Beyond the Standard Model (BSM) [1–10]. Given the expected experimental data sets, this distribution will be measured both inclusively and in association with jets up to several hundreds of GeV in the Higgs transverse momentum [11, 12]. Already now experimental measurements by ATLAS and CMS yield sensitivity up to few hundred GeV [13, 14].

Both in the inclusive case and for the production in association with jets, the dominant Higgs production mode in the SM originates via a top-quark loop in gluon-gluon fusion, however, at large transverse momentum eventually also vector-boson fusion (VBF), Higgsstrahlung (VH) and top-pair associated Higgs production contribute significantly [15]. For the production in association with jets, additional constraints on jet invariant masses and/or rapidities allow the relative fraction of the VBF events to be enhanced [16, 17]. Precise VBF measurements will allow us to constrain on the one hand the electroweak (EW) couplings of the Higgs, and on the other hand when restricting to large Higgs transverse momentum they

will allow for complementary constraints on models of new physics [18–23]. In this regard, one of the dominant uncertainties in VBF measurements originates from the background modelling of the gluon-induced Higgs production mode.

The loop-induced nature of the gluon-gluon fusion Higgs production process makes higher-order corrections notoriously difficult to calculate. In QCD fixed-order perturbation theory including mass effects, inclusive Higgs production at next-to-next-to-leading order (NNLO) was calculated only very recently [24], Higgs plus jet production is known at next-to-leading order (NLO) [25–28], while Higgs plus dijet production (and beyond) is only known at leading order (LO) [29–33] with parton shower effects to estimate higher order corrections [34]. In the NLO computations of Higgs plus jet production the crucial two-loop virtual contributions have been obtained numerically [35, 36] in refs. [25, 28] respectively via a suitable high-energy expansion [37] in refs. [26, 27].

Formally, below the top-quark threshold, higher precision can be achieved via the heavy top loop (HTL) approximation, effectively integrating out the top-quark loop [38]. In the HTL approximation, inclusive Higgs production is known at N3LO [39–44], Higgs plus jet production at NNLO [45–49], and Higgs plus dijet production at NLO [50, 51] (for Higgs plus trijet production see [52]). For inclusive Higgs production and for $p_{\mathrm{T,H}} < m_t$ (where m_t is the top-quark mass) predictions in the full SM and in the HTL agree at the percent level. For $p_{\mathrm{T,H}} \ll m_t$ eventually fixed-order perturbation theory becomes unreliable and a matching to higher logarithmic accuracy becomes mandatory [53–59], and also bottom-quark effects have to be considered [60–66].

At the other end of the spectrum, for $p_{\mathrm{T,H}} > m_t$, the accuracy of the HTL quickly deteriorates due to a different high-energy scaling compared to the full theory [67]. For $p_{\mathrm{T,H}} = 500(1000)\,\mathrm{GeV}$ the two differ by a factor of about 4(10). In this high-energy regime in order to improve with respect to the HTL additional $\mathcal{O}(1/m_t)$ corrections have been investigated [31, 68, 69]. Overall, the above cited explicit fixed-order computations have shown that higher-order corrections computed in the HTL rescaled with lower-order predictions with explicit mass dependence yield remarkably good approximations of the full result despite the fact that the HTL is not valid in this energy regime. Therefore, it appears to be justified to tentatively apply this very same procedure also at the highest perturbative orders, where validation of the approximation is not yet possible. An example of such an approximation at the currently highest available perturbative order is presented in ref. [15] for Higgs plus jet production where NNLO corrections in the HTL are combined with NLO corrections in the full SM. However, defining a reliable uncertainty on such approximations remains crucial. Such approximations of reweighting higher-order computations in the HTL with exact lower order results are also at the basis of all currently available NLO Monte Carlo predictions matched to parton showers for Higgs plus (multi-)jet production [34, 70–73].

In this paper we present fixed-order NLO QCD computations for $pp \to H + j$ and also $pp \to H + jj$ including top-quark mass effects. The computation for $pp \to H + j$ continues the study of ref. [25], i.e. two-loop virtual corrections in the full SM are evaluated numerically via SECDEC-3 [35, 36]. Here we present additional kinematic observables besides the $p_{\mathrm{T,H}}$ distribution already shown in ref. [25] and compare the relative higher-order corrections in the full SM against the HTL, and also an alternative approximation known as

FT$_{\text{approx}}$, which has been introduced in ref. [74] in the context of calculations for multi-Higgs production. In the FT$_{\text{approx}}$ all ingredients of the NLO computation are computed exactly, except for the two-loop virtual contributions, which are approximated in the HTL and reweighted with LO mass dependence. In the case of $pp \to H + jj$ production we compare results in the HTL and in the FT$_{\text{approx}}$, as the exact five-point two-loop virtual amplitudes remain beyond current technology. The main aim of this study is three-fold: firstly, we would like to offer complementary kinematic information for the $pp \to H + j$ process, while also offering a (partial) validation of the results already presented in ref. [25]. In this respect, the present study uncovered an issue affecting the real corrections included in ref. [25], which has subsequently been rectified. Secondly, we would like to investigate the $pp \to H + jj$ process in a kinematic regime relevant for VBF analyses. The comparison of NLO/LO ratios (usually known as K-factors) among HTL, FT$_{\text{approx}}$ and the full SM will help to put results obtained in a reweighted HTL on a more solid footing. Thirdly, results presented in this study can be seen as an intermediate step towards an NNLO computation of $pp \to H + j$ including exact mass effects wherever possible.

Technically, the computations of the NLO corrections to $pp \to H + j$ and $pp \to H + jj$ production are performed within the NNLOJET fixed-order Monte Carlo framework, which employs antenna subtraction for the handling of infrared (IR) singularities [75–83]. All loop-squared amplitudes are evaluated via a new interface between NNLOJET and OPENLOOPS2 [84–86] based on the latest (soon to be released) version OPENLOOPS2.2 which in turn implements a new reduction method called *Otter* [87], which ensures excellent numerical stability in particular of the loop-induced real radiation amplitudes deep into the unresolved regime. We will investigate and discuss this numerical stability issue explicitly.

The structure of the paper is as follows. In section 2 we describe the computational setup and employed tools. Numerical results for H+jet and H+2 jets production will be presented in section 3. We will conclude in section 4.

2 Analysis framework and tools

In this paper, we present predictions for the production of a boosted Higgs boson in the gluon-fusion channel. We consider Higgs bosons produced in association with one ($pp \to H + j$) or two ($pp \to H + jj$) jets with NLO QCD corrections and include the effects of a finite top-quark mass either fully or via a suitable approximation. For $pp \to H + j$ we compute the transverse momentum distribution of the Higgs boson including a finite top-quark mass, which has appeared previously in the literature [25–28], as well as the Higgs boson plus jet invariant mass distribution. For $pp \to H + jj$, the virtual corrections involve two-loop amplitudes for $2 \to 3$ scattering. The mathematical complexity of the virtual corrections makes their computation currently intractable using either numerical or analytical methods. We therefore adopt an approximation scheme to the full theory (FT$_{\text{approx}}$) [74, 88] for the NLO QCD corrections to Higgs boson plus two jet production. Specifically, we include the exact top-quark mass dependence (SM) in the real corrections and infrared singular subtraction terms while using the virtual corrections in the heavy top-quark limit (HTL) re-weighted by the full Born level contribution on an event-by-event basis. In fact, although

the full matrix elements relevant to the virtual contributions of H + 2 jets production are currently not available, nevertheless, their explicit infrared divergence at NLO can be predicted by the Catani dipole structure [89]:

$$\text{Pole}\{|\mathcal{M}_4^2(m_t, \mu_R^2; \{p\})|^2\} = \sum \boldsymbol{I}^{(1)}(\epsilon, \mu_R^2; \{p\})|\mathcal{M}_4^1(m_t; \{p\})|^2, \tag{2.1}$$

where m_t is the top-quark mass, μ_R^2 is the renormalisation scale, $\{p\}$ is the momentum set regarding all external particles, $|\mathcal{M}_n^m|^2$ is the matrix element with n legs and m loops and $\boldsymbol{I}^{(1)}(\epsilon, \mu_R^2; \{p\})$ is the dipole operator containing all explicit IR divergences in d space-time dimensions. The explicit expressions for dipole operators at squared matrix element level can be found in [75]. We estimate the finite contribution of $|\mathcal{M}_4^2(m_t, \mu_R^2; \{p\})|^2$ by re-weighting the corresponding matrix element in the HTL approximation ($m_t \to \infty$) using:

$$|\mathcal{M}_4^2(m_t, \mu_R^2; \{p\})|^2 \to |\mathcal{M}_4^1(\infty, \mu_R^2; \{p\})|^2 \frac{|\mathcal{M}_4^1(m_t; \{p\})|^2}{|\mathcal{M}_4^0(\infty; \{p\})|^2}. \tag{2.2}$$

Consequently, eq. (2.2) also recovers the explicit pole structure in eq. (2.1).

The FT$_{\text{approx}}$ prediction has proved to be remarkably reliable for Higgs plus one jet [49] production and, to a lesser extent, di-Higgs [90] production (however in the latter case, it is much less reliable for differential distributions) at the LHC. Comparing the FT$_{\text{approx}}$ and SM results for Higgs plus one jet production, the updated version of the study in [25] reports better than 1% agreement for the fiducial cross section and in general 5% agreement for the Higgs transverse momentum distribution up to 1 TeV when including NLO QCD corrections. Here we confirm this excellent agreement. In fact, the FT$_{\text{approx}}$ prediction is identical to the full top-quark mass dependent one at NLO except for the difference in the finite contribution of the virtual matrix elements described in eq. (2.2). In order to quantify this difference, we examine, on an event-by-event basis, the ratio of the difference between the virtual contributions to the full born contribution,

$$\mathcal{D}_{\text{B}}^{\text{V}}(m_t, \mu_R^2; \{p\}) = \frac{|\mathcal{M}_4^2(m_t, \mu_R^2; \{p\})|^2}{|\mathcal{M}_4^1(m_t; \{p\})|^2} - \frac{|\mathcal{M}_4^1(\infty, \mu_R^2; \{p\})|^2}{|\mathcal{M}_4^0(\infty; \{p\})|^2}. \tag{2.3}$$

Note that the ratio of the approximated and full finite virtual contributions would be an IR-subtraction scheme dependent quantity, whilst the difference is independent of the scheme choice. For the phase-space region and the scale choices we consider (in section 3.1), we find the size of $\mathcal{D}_{\text{B}}^{\text{V}}$ in the dominant gluon-gluon contribution is at the 1–2% level for the majority of the phase-space points, increasing to $\sim$10% only for points with large m_{Hj} and intermediate p_T^H. For the quark-gluon channels we observe that $\mathcal{D}_{\text{B}}^{\text{V}}$ is at the 2% level at low $p_{\text{T,H}}$, increasing to up to 14% above the top-quark threshold. For the quark-quark channel, the full center-of-mass energy flows into the gluon-gluon-Higgs vertex (i.e. this is an s-channel production process), consequently this channel has a pronounced behaviour close to and above the top threshold which is not captured by the approximation, leading to large differences between the HTL and full theory, with $\mathcal{D}_{\text{B}}^{\text{V}}$ increasing up to 100%. With additional jets in the final state, the agreement in the quark-quark channel is expected to improve due to additional contributions from the $t-$ and u-channels. Weighting each

channel by its corresponding PDF luminosity the net effect results in $\mathcal{D}_{\mathrm{B}}^{\mathrm{V}}$ being less than 5% for the majority of the events, reaching up to $\sim 10\%$ in suppressed phase-space regions. This is consistent with the NLO/LO K-factors shown in section 3.3. We therefore consider the $\mathrm{FT}_{\mathrm{approx}}$ scheme reliable with respect to the precision at NLO QCD and implement the first application of this approximation to Higgs boson plus two jet production at NLO in QCD.

In the following sections we document the detailed implementation of our calculations. The NNLOJET program is used as a parton level event generator and all Born and real radiation one-loop contributions are computed using OpenLoops2.2. The two-loop matrix elements involving a finite top-quark mass for $pp \to H + j$ are computed exactly using SecDec-3.

2.1 Parton level event generator: NNLOJET

NNLOJET is a parton-level event generator equipped with flexible histogram analysis tools and scattering matrix elements evaluated in both the HTL approximation and in the full SM. It implements the antenna subtraction method to cancel infrared singularities from higher order QCD corrections [75–83] while retaining the fully differential information of final state particles.

In this study, we combine NNLOJET with loop induced matrix elements provided by OpenLoops2 and SecDec-3 to study finite top-quark mass corrections for H+jet and $H + 2$ jets production with NLO QCD corrections. The HTL and SM have the same infrared singular behaviour for both real emissions and virtual corrections, the antenna subtraction method can therefore be readily applied to regulate infrared singularities at NLO for loop-induced processes. Schematically, the fully differential NLO contribution takes the form:

$$
\begin{aligned}
\mathrm{d}\sigma_{H+n\mathrm{jet}}^{\mathrm{NLO}} = \int_{\mathrm{d}\Phi_{n+1}^H} &\left[|\mathcal{M}_{n+3}^1(m_t; \{p\})|^2 - \sum_{\{p\}} X_3^0 |\mathcal{M}_{n+2}^1(m_t; \{\tilde{p}\})|^2 \right] \\
+ \int_{\mathrm{d}\Phi_n^H} &\left[|\mathcal{M}_{n+2}^2(m_t, \mu_R^2; \{p\})|^2 + \sum_{\{p\}} \mathcal{X}_3^0 |\mathcal{M}_{n+2}^1(m_t; \{p\})|^2 \right],
\end{aligned}
\tag{2.4}
$$

where Φ_n^H is the final state phase space of one Higgs plus n partons, X_3^0 represents the tree-level three-parton antenna functions, $\mathcal{X}_3^0$ represents the corresponding integrated antenna functions in d-dimensions and $\{\tilde{p}\}$ is the momentum set after antenna mapping with one less parton compared to the $\{p\}$ momentum set. We use X_3^0 and the corresponding reduced matrix elements ($|\mathcal{M}_{n+2}^1|^2$) to capture the infrared singular behaviour of real radiations in $|\mathcal{M}_{n+3}^1|^2$, leading to a infrared finite contribution of the first bracket in eq. (2.4). By adding back the integrated antenna functions $\mathcal{X}_3^0$ in the second bracket of eq. (2.4), we render the integrand over the Φ_n^H phase space IR finite. The explicit IR divergences (which appear as poles in the regulator ϵ) cancel analytically with the explicit IR poles from the virtual contribution ($|\mathcal{M}_{n+2}^2|^2$). In $\mathrm{FT}_{\mathrm{approx}}$, one replaces the virtual contribution in the second bracket of eq. (2.4) according to eq. (2.2) and the explicit pole cancellation is automatically retained.

2.2 One-loop contributions: OPENLOOPS2.2

All one-loop amplitudes contributing at the Born and real radiation level are provided by the OPENLOOPS2.2 package, an upcoming improved version of the OPENLOOPS2 program which implements a new reduction method called *Otter* [87]. Compared to the original algorithm [84], OPENLOOPS2 includes significant improvements in numerical stability and performance for the computation of tree-loop interference amplitudes. These improvements were achieved by a combination of the so-called on-the-fly reduction algorithm [85] and an automated stability system. However, the current implementation, which was designed for tree-loop interferences, cannot be directly applied to loop-induced amplitudes, such as those required for the present computation. In OPENLOOPS2.2 a new tensor integral reduction method has been developed, based on the on-the-fly reduction algorithm [85], that can also be used for loop-squared amplitudes. It profits from recent improvements in performance and methods developed for handling numerical instabilities. More specifically, numerical instabilities are avoided by using certain freedoms in the selection of the reduction identities, and analytical any-order expansions of three-point tensor integrals in the limit of small Gram determinant [86]. Furthermore, within OPENLOOPS2.2 residual instabilities are captured by a rescaling test and tensor integrals are recomputed in quadruple precision in case the given accuracy is not reached. This upgrade to quadruple precision is efficient, and also important for computations in deep infrared regions. OPENLOOPS2.2 depends on COLLIER [91] only for double precision scalar integrals and on ONELOOP [92] for quadruple precision scalar integrals.

Numerical stability. The numerical stability of OPENLOOPS2.2 is crucial for the calculations of H+jet and H + 2 jets productions presented in this paper, especially to contributions from infrared kinematical regions, which are numerically challenging. In figure 1 we illustrate as a benchmark the stability of the critical gg → Hgg and gg → Hggg amplitudes subject to single soft or collinear radiation. The degree of softness and collinearity are defined as

$$\xi_{\rm soft} = E_{\rm soft}/\sqrt{s}, \quad \xi_{\rm coll} = \theta_{ij}^2, \tag{2.5}$$

where $E_{\rm soft}$ is the energy of the soft particle, and θ_{ij} denotes the angle of the collinear branching. The numerical stability is defined as

$$\mathcal{A} = \log_{10}\left(\frac{\mathcal{W} - \mathcal{W}^{(0)}}{\mathcal{W}^{(0)}}\right), \tag{2.6}$$

where $\mathcal{W}$ denotes the one-loop-squared matrix element, $\mathcal{W}^{(0)}$ is the benchmark result, and $\mathcal{A}$ corresponds to the number of stable digits up to a minus sign. As can be seen from these plots, the numerical accuracy remains very high all the way down to the deep infrared regime.

Numerical performance. In table 1 we present results for the average evaluation time of samples of random phase-space points using various different modes/versions of OPENLOOPS. In particular, here certain parts of the amplitude are evaluated in double or in quadruple precision, or a realistic error estimate of the amplitudes is performed. In summary, performance is greatly improved in OPENLOOPS2.2 which in particular makes a tensor integral based
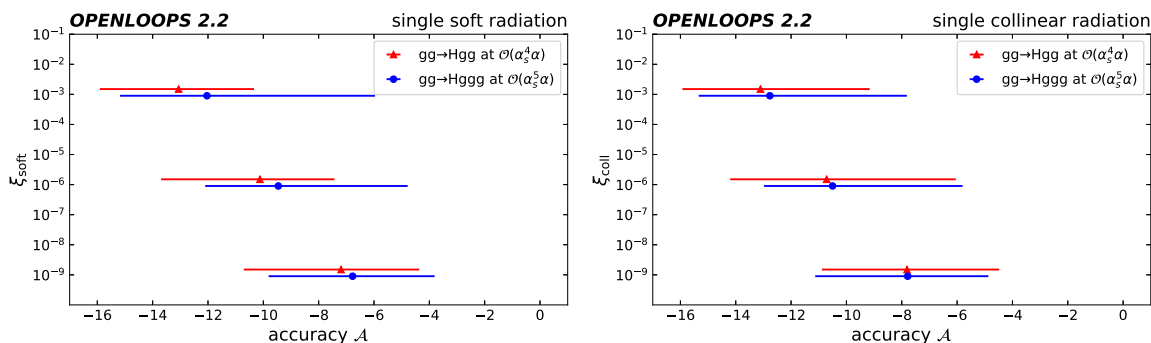
Figure 1. Stability plots in IR regions for one-loop-squared matrix elements in gg $\to$ Hgg and gg $\to$ Hggg versus the degree of collinear $\xi_{\rm coll}$ or soft $\xi_{\rm soft}$ singularity obtained with OPENLOOPS2.2. For each value of $\xi_{\rm soft/coll}$, the numerical accuracy is calculated with a sample of 10^3 randomly distributed infrared events. Unstable points are detected by a rescaling test and rescued if the relative accuracy of 10^{-6} is not reached. The rescue step reevaluates the tensor integrals to quad precision. The accuracy of the so-obtained value is determined by comparing it to a quadruple precision benchmark whose accuracy is also assessed by a rescaling test. The plotted central points and variation bands correspond, respectively, to the average and 100% confidence interval of $\mathcal{A}$.

rescaling test cheap. Moreover, since OPENLOOPS2.2 operates also in quadruple precision with very high numerical efficiency, numerically unstable points can be rescued in a reliable way, which has largely been prohibitive for loop-squared amplitudes in OPENLOOPS2. In fact, OPENLOOPS2.2 allows for rescue of unstable points in a new hybrid mode, where only the tensor integrals are evaluated in higher numerical precision resulting in a 8-fold and 3-fold increase in runtime compared to pure double precision for $gg \to Hgg$ and $gg \to Hggg$ respectively, compared to a roughly 80-fold increase in runtime for full quadruple precision. In practice, and as used for the present computation of this paper in OPENLOOPS2.2 a combination of pure double precision with this new hybrid mode is used. Based on a pure double precision evaluation the stability for every phase-space point is estimated based on a rescaling test of only the tensor integrals. Then, only for critical points the tensor integrals are reevaluated in quadruple precision based on the hybrid mode.

2.3 Two-loop contributions: SECDEC-3

For $pp \to H + j$ production, we evaluate the two-loop virtual contributions with exact top-quark mass dependence as presented in refs. [25, 28]. Briefly, the two-loop amplitudes, which depend on four mass scales (the Mandelstam invariants s and t as well as the two masses m_t and m_h), are expressed in terms of a basis of master integrals using the program REDUZE2 [93]. In order to obtain the integral reduction in a reasonable time and to reduce the size of the resulting amplitude, the ratio of the Higgs boson mass to the top-quark mass is fixed according to $m_H^2/m_t^2 = 12/23$. The master integrals are then sector decomposed using the program SECDEC-3 [35, 36] and numerically integrated on Graphics Processing Unit (GPUs) using the Quasi-Monte Carlo method [94, 95]. To improve the stability of the amplitude we select a quasi-finite basis of master integrals as outlined in ref. [28], this differs from the basis originally used in ref. [25]. We observe that the new choice of master

Mode	$gg \rightarrow Hgg$ (time/psp)	$gg \rightarrow Hggg$ (time/psp)
OL2.1+Collier DP	13ms	0.56s
OL2.1+Collier DP + error estimation	19ms	0.89s
OL2.1+CutTools QP	43000ms	2300s
OL2.2+Otter DP	8.9ms	0.29s
OL2.2+Otter DP + error estimation	11ms	0.32s
OL2.2+Otter DP+QP tensor integrals	68ms	0.87s
OL2.2+Otter QP	740ms	23s

Table 1. Runtimes for loop-squared amplitudes for $gg \rightarrow Hgg$ and $gg \rightarrow Hggg$ in OPENLOOPS. All numbers have been produced on an Intel(R) Core(TM) i7-7700 CPU @ 3.60GHz. The first three rows correspond to the modes so far available in OPENLOOPS2 [86]. These employ double precision evaluation with COLLIER (first and second row), where in the second row tensor integrals are computed twice using the COLI and DD branches of COLLIER in order to obtain an error estimate. The third row employs CUTTOOLS and the entire amplitude is evaluated in quadruple precision. For the amplitudes at hand the resulting runtimes in quadruple precision are prohibitive to be used as rescue system. The lower four rows represent evaluation based on the new *Otter* method in OPENLOOPS2.2. In this case the error estimation is performed via a rescaling test where all tensor integrals are recomputed with rescaled kinematics. The sixth row corresponds to a new hybrid mode where only the tensor integrals are evaluated in quadruple precision, and everything else in double precision. The last row shows the performance for a full quadruple precision evaluation within OPENLOOPS2.2.

integrals also significantly reduces the complexity of the coefficients of the master integrals appearing in the amplitude and thus the size of the code.

The results presented here are produced using a total of 6497 phase-space points for the two-loop virtual contribution. In ref. [25], a fraction of the phase-space points were distributed such that they provide a good estimate of the total cross section (assuming a jet cut of $p_{T,j} > 30\,\text{GeV}$) and additional phase-space points were generated to sample the tail of the $p_{T,H}$ distribution. We reuse these existing phase-space points and also compute an additional 1007 points to populate the large invariant mass region m_{Hj} for $p_{T,j} > 300\,\text{GeV}$.

3 Numerical results

3.1 Setup

As an extension of the study of Higgs plus one jet production at NLO [25], we adopt the same input parameters and numerical setup in the current calculation. To quantify the impact of increasing the number of final state jets, we keep the input parameters consistent between H+jet and $H + 2$ jets production. The counting of the number of jets in this study is inclusive. There is no difference between inclusive and exclusive jet counting for LO while results at NLO accuracy receive contributions from real emissions including events classified with one addtional jet. For the Higgs and top-quark mass we use $m_H = 125\,\text{GeV}$ and $m_t = 173.055\,\text{GeV}$. The top-quark Yukawa coupling $\lambda_t = \sqrt{2}m_t/v$ is determined by

the vacuum expectation value (vev) of the Higgs $v = \frac{M_W \sin \theta_W}{\sqrt{\pi}\alpha_{\text{QED}}} = 246.219\,\text{GeV}$ and the top-quark mass. We use the five flavour scheme assuming light quarks are massless in both inital and final states.

Throughout our calculation, the top-quark mass is renormalised using the on-shell (or pole mass) scheme. It has been pointed out in the literature that several Higgs boson production processes (including Higgs boson production in association with jets) are sensitive to the scheme and scale used to renormalise quark masses [96–99]. For example, at LO, the difference between the pole mass scheme and the $\overline{\text{MS}}$ scheme at scale $m_{H,j}/2$ was found to be around 12% for $m_{H,j} = 700\,\text{GeV}$ and $p_{T,j} > 300\,\text{GeV}$. At larger $p_{T,H}$ the difference between the two schemes grows and can reach $\approx 25\%$ for $p_{T,H} = 1\,\text{TeV}$. In off-shell Higgs boson production, off-shell Higgs boson decay to photons and in Higgs pair production, the NLO corrections reduce the mass scheme uncertainty to approximately half that of the LO [96, 99]. By analogy, we may expect that the mass scheme uncertainty, which we do not assess, is similar in size to our NLO scale uncertainties (see below).

We employ the PDF4LHC15_nlo_30_pdfas PDF set [100] throughout and all of our predictions are at a center of mass energy of $\sqrt{S} = 13\,\text{TeV}$. Renormalisation and factorisation scales are chosen as

$$\mu_{\text{R,F}} = \xi_{\text{R,F}} \cdot H_T/2, \quad \text{with} \quad H_T = \sqrt{m_H^2 + p_{\text{T,H}}^2} + \sum_j |p_{\text{T,j}}|, \tag{3.1}$$

where the sum includes all final state partons. Our central scale corresponds to $\xi_{\text{R,F}} = (1,1)$ and we determine scale uncertainties via the standard 7-point factor-2 variations $\xi_{\text{R,F}} = (2,2), (2,1), (1,2), (1,1), (1,\frac{1}{2}), (\frac{1}{2},1), (\frac{1}{2},\frac{1}{2})$). Any reconstructed jets are clustered via the anti-k_t [101] algorithm with $R = 0.4$. We apply the following cuts:

$$H + \text{jet}: \quad p_{\text{T,j}} > 30\,\text{GeV}, \tag{3.2}$$

$$H + 2\,\text{jets}: \quad p_{\text{T,j}_1} > 40\,\text{GeV} \text{ and } p_{\text{T,j}_2} > 30\,\text{GeV}. \tag{3.3}$$

The latter asymmetric jet cuts avoid a perturbative instability in the limit $p_{\text{T,H}} \to 0\,\text{GeV}$.

3.2 Fiducial total cross sections

Applying the computational setup in section 3.1, we document the fiducial total cross section for H+jet and $H + 2\,\text{jets}$ produciton in table 2. For reference we present results for the HTL, FT$_{\text{approx}}$ and SM predictions. We also include the fiducial total cross section for boosted Higgs with $p_{T,H} > 300\,\text{GeV}$. Further fiducial cross sections with varying $p_{T,H}$ cuts are listed in appendix A. The numbers for H+jet reported here agree, within the statistical uncertainty, with the updated version of ref. [25].

Together with predictions obtained with the central scale defined in eq. (3.1) we show the upper and lower values obtained by the envelope of 7-point scale variations. For H+jet production without the fiducial constraint of $p_{T,H}$, the top-quark mass effects lead to an increase of 4.3% (4.6%) at LO (NLO) comparing to HTL. There is an increase of about 1% in the total NLO cross section when comparing the FT$_{\text{approx}}$ result with the full top-quark mass dependence. The NLO/LO K-factor is consistent among HTL, FT$_{\text{approx}}$ and SM at about 1.65.

$\sigma[\text{pb}]$		Inclusive $p_{T,H}$			$p_{T,H} > 300\,\text{GeV}$		
		LO	NLO	K	LO	NLO	K
H+jet	HTL	$8.22^{+3.17}_{-2.15}$	$13.57^{+2.11}_{-2.09}$	1.65	$0.086^{+0.038}_{-0.024}$	$0.160^{+0.033}_{-0.030}$	1.86
	$\text{FT}_{\text{approx}}$	$8.56^{+3.30}_{-2.24}$	$14.06(1)^{+2.17}_{-2.16}$	1.64	$0.046^{+0.020}_{-0.013}$	$0.088^{+0.019}_{-0.017}$	1.91
	SM	$8.56^{+3.30}_{-2.24}$	$14.15(7)^{+2.29}_{-2.21}$	1.65	$0.046^{+0.020}_{-0.013}$	$0.089(3)^{+0.020}_{-0.017}$	1.93
H + 2 jets	HTL	$2.87^{+1.67}_{-0.99}$	$4.33^{+0.59}_{-0.80}$	1.51	$0.120^{+0.071}_{-0.042}$	$0.160^{+0.012}_{-0.025}$	1.33
	$\text{FT}_{\text{approx}}$	$2.92^{+1.70}_{-1.01}$	$4.45(1)^{+0.63}_{-0.83}$	1.52	$0.068^{+0.040}_{-0.024}$	$0.092^{+0.008}_{-0.015}$	1.35
	SM	$2.92^{+1.70}_{-1.01}$	$-$	$-$	$0.068^{+0.040}_{-0.024}$	$-$	$-$

Table 2. Integrated cross sections at LO and NLO in the HTL and $\text{FT}_{\text{approx}}$ approximations and with full top-quark mass dependence (SM) for H+jet and H+2 jets production together with corresponding K-factors. Uncertainties correspond to the envelope of 7-point scale variations. For H+jet production we require $p_{T,\text{j}} > 30\,\text{GeV}$, while for H + 2 jets production we require $p_{T,\text{j}_1} > 40\,\text{GeV}$, $p_{T,\text{j}_2} > 30\,\text{GeV}$. On the left no further phase-space restrictions are considered, while on the right we additionally require $p_{T,H} > 300\,\text{GeV}$. Numerical integration errors larger than permil level are indicated in brackets.

With the fiducial constraint of $p_{T,H}$ larger than $300\,\text{GeV}$, we observe a similar amount (2.3%) of relative increase from the $\text{FT}_{\text{approx}}$ prediction to the result with full top-quark mass effects at NLO. In contrast, the HTL prediction is 78% (81.8%) larger than the full theory ($\text{FT}_{\text{approx}}$) result due to large logarithmic corrections from the disparity in scales between m_t^2 and $p_{T,H}^2$. The NLO/LO K-factor for $p_{T,H} > 300\,\text{GeV}$ is however again almost universal among HTL, $\text{FT}_{\text{approx}}$ and SM at about 1.9. To be precise, the K-factor in the full SM is 5.3% resp. 2.6% larger compared to the HTL and $\text{FT}_{\text{approx}}$ predictions.

For H+2 jets production without the fiducial constraint on $p_{T,H}$, the $\text{FT}_{\text{approx}}$ prediction induces a 1.7% (2.8%) increase compared the HTL approximation at LO (NLO). Considering the fiducial constraint of $p_{T,H}$ larger than $300\,\text{GeV}$, the HTL fiducial total cross section is about 1.76 (1.74) times the $\text{FT}_{\text{approx}}$ predictions at LO (NLO). However, again in both selections NLO K-factors are universal with mass corrections in the $\text{FT}_{\text{approx}}$ below the 2% level.

For the absolute cross sections the extra jet emission in H + 2 jets production decreases the total H+jet cross section by more than a factor of 3 from 14.06 pb (H+jet) to 4.45 pb considering the $\text{FT}_{\text{approx}}$ predictions at NLO in both cases. In contrast, in the boosted Higgs boson regime, the total NLO cross sections are comparable, while the NLO K-factor is about 46% larger in the H+jet computation compared to the H + 2 jets one. This can be understood from the restriction to the back-to-back configuration in the H+jet computation at LO. Multi-jet configurations recoiling against the hard Higgs only open up at NLO, where they are effectively described at LO. In contrast in the H + 2 jets computation such configurations already contribute at LO.

In order to quantify top-quark mass effects in various fiducial regions and to explore the possibility to extrapolate the mass effect to higher order corrections, in the following sections we present in-depth comparisons of differential cross sections for H+jet and H+2 jets production.
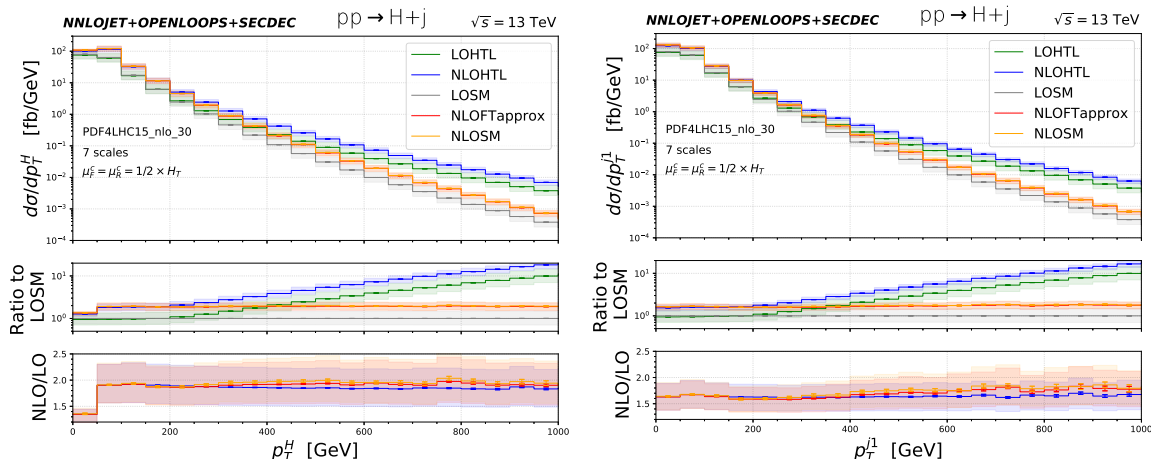
Figure 2. Transverse momentum distribution of the Higgs (left) and the hardest jet (right) in H+jet production. We show LO predictions in the full SM (LOSM, magenta) and the HTL (LOHTL, green) as well as NLO predictions in the HTL (NLOHTL, blue), the FT$_{\text{approx}}$ (NLOFTapprox, red) and the full SM (NLOSM, orange). The upper panel shows absolute predictions. The first ratio plot shows corrections with respect to LOSM, while the second ratio plot shows NLO corrections normalised to the respective LO prediction, i.e. NLOHTL/LOHTL, NLOSM/LOSM, and NLOFTapprox/LOSM. Shaded bands correspond to scale variations. Error bars indicate integration uncertainties.

3.3 Fiducial differential cross sections for H+jet production

In figures 2–3 we present numerical results for H+jet production at the LHC with $\sqrt{S} = 13$ TeV. We compare NLO corrections in the HTL with the FT$_{\text{approx}}$ approximation, and with the full SM.

In figure 2 we consider the transverse momentum distribution of the Higgs on the left and of the jet on the right. These distributions are identical at LO, and are also highly correlated at NLO. As is well known, for $p_{T,X} > m_t$ $(X = H, j)$ the HTL approximation breaks down and predicts a very different high-energy scaling compared to the SM. However, for NLO/LO ratios in the bottom panels of figure 2, at least at the $O(10\%)$ level, higher-order QCD corrections in the HTL agree well with the FT$_{\text{approx}}$ and the full SM. Further improvement of agreement is observed between the FT$_{\text{approx}}$ and the full SM at the $O(5\%)$ level within numerial uncertainties. The scale variation bands in the ratio plots are obtained by fixing the observable at the central scale choice in the denominator while taking the envelope of scale choices in the numerator by the 7-point factor-2 variations. We observe consistent agreement for the size of scale variations also for the ratio plots. In $p_{T,H}$ the corrections are at the level of 90–110%, while in $p_{T,j}$ they are at the level of 60–80%, for the entire considered range, i.e shape corrections are mild. Examining the corrections in more detail an overall increase of the corrections of $\approx$ 5–10% can be appreciated for the full SM compared to the HTL, with a mild relative increase at large transverse momenta slightly larger for $p_{T,j}$ than for $p_{T,H}$. Corrections in the FT$_{\text{approx}}$ and the HTL agree exactly up to $p_{T,H}/p_{T,j} \sim m_t$. Beyond that, corrections in the FT$_{\text{approx}}$ are a few percent larger compared to the HTL, with again a very slight increase at large transverse momenta. The remaining scale uncertainties at NLO are at the 20–25% level throughout.
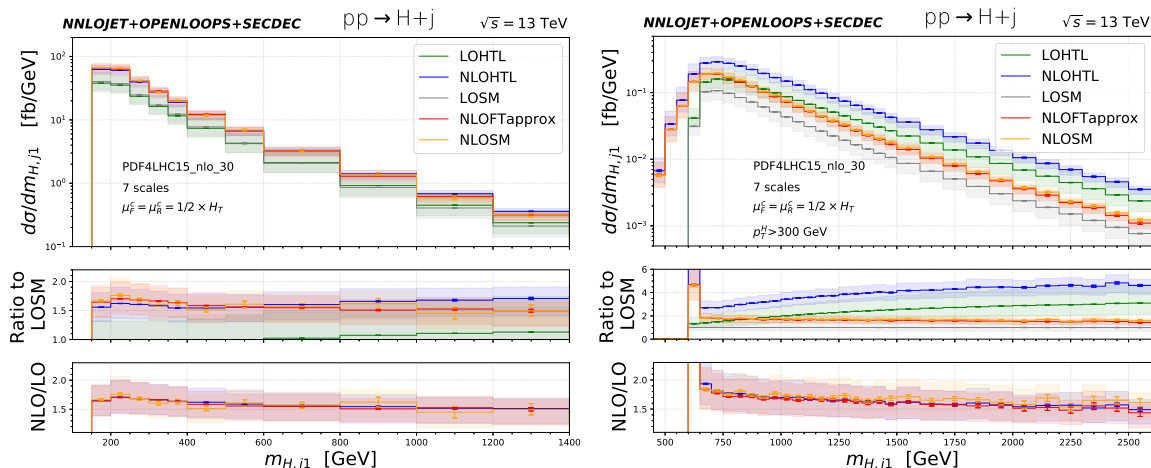
Figure 3. Invariant mass distribution of the Higgs and the jet for inclusive H+jet production (left) and with $p_{T,H} > 300\,\text{GeV}$ (right). Colour coding and labelling as in figure 2.

In figure 3 we turn to a different kinematic regime in H+jet production by considering invariant mass distributions in the Higgs-jet system on the left for inclusive H+jet production and on the right considering $p_{T,H} > 300\,\text{GeV}$. For the inclusive m_{Hj} distribution the HTL NLO result increases mildly by 10–20% in the tail of the distribution compared to the FT$_{\text{approx}}$ and the full SM. However, the NLO K-factor is universal in all three predictions decreasing from about 1.7 at small m_{Hj} to about 1.5 at large m_{Hj} with similar relative size of scale variation. Finally, in the exclusive $p_{T,H} > 300\,\text{GeV}$ phase-space absolute predictions in the HTL and FT$_{\text{approx}}$ diverge for increasing m_{Hj}. However, also here the relative NLO corrections are found to be largely identical for the HTL, FT$_{\text{approx}}$ and full top-quark mass results. This holds at large m_{Hj} as well as at small m_{Hj}, which for $m_{Hj} < 600\,\text{GeV}$ is kinematically inaccessible at LO due to the $p_{T,H} > 300\,\text{GeV}$ requirement.

From the detailed comparison of $p_{T,H}$, $p_{T,j}$ and m_{Hj} distributions of H+jet production, we observe excellent agreement of differential NLO/LO K-factors (for the central scale and scale variations) among theory predictions using HTL, FT$_{\text{approx}}$ and the exact top-quark mass dependence. This observation validates the multiplicative reweighting procedure introduced in [49] at histogram level and further strengthens the reweighed predictions for H+jet production at NNLO accuracy [15].

3.4   Fiducial differential cross sections for H + 2 jets production

In figures 4–7 we turn to the numerical results for H + 2 jets production. We compare NLO corrections in the HTL with the FT$_{\text{approx}}$ approximation, focussing on multi-jet observables and jet correlations with and without boosted Higgs kinematics (i.e. inclusive and with an additional $p_{T,H} > 300\,\text{GeV}$ requirement). As discussed in the introduction these are phenomenologically highly relevant for the modelling of H + 2 jets backgrounds in analyses for VBF Higgs production.
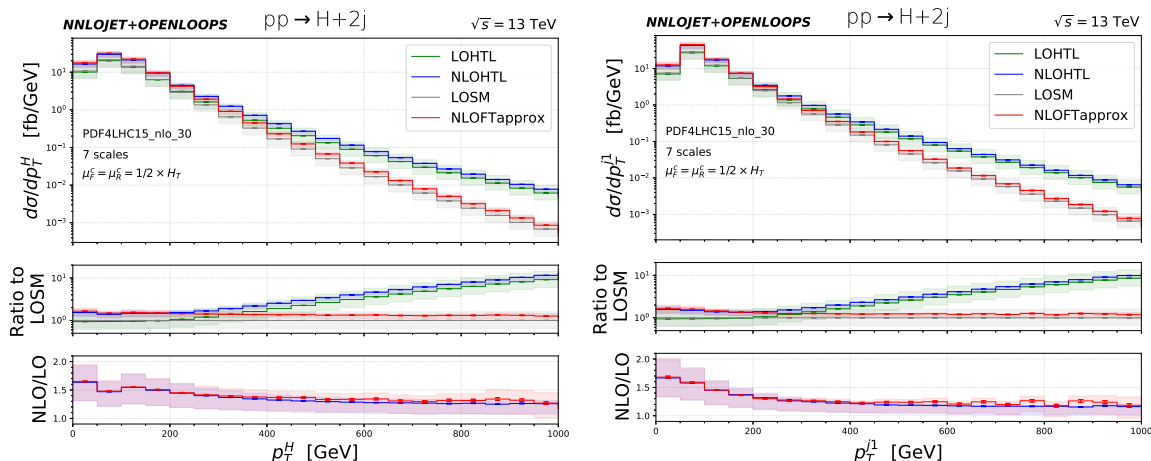
Figure 4. Transverse momentum distribution of the Higgs (left) and the hardest jet (right) in H + 2 jets production. Colour coding and labelling as in figure 2.

In figure 4 we consider the transverse momentum of the Higgs (left) and of the hardest jet (right). These plots can directly be compared with the corresponding ones for H+jet production in figure 2. Again we observe very large deviations of the nominal predictions at large transverse momenta. At the same time also the QCD corrections are sizeable: around 60–70% at small p_T and around 30% for $p_{T,H}/p_{T,j} = 1\,\mathrm{TeV}$. However the relative NLO corrections normalised to the respective LO show a universal behaviour, i.e. they are identical in the HTL and the $\mathrm{FT}_{\mathrm{approx}}$.

A similar picture as for the transverse momentum distributions emerges when looking at the distribution in the invariant mass of the Higgs and the hardest jet, as depicted in figure 5. Both, for the inclusive selection (as shown on the left), and for the boosted Higgs selection with an additional $p_{T,H} > 300\,\mathrm{GeV}$ requirement, the QCD corrections in the $\mathrm{FT}_{\mathrm{approx}}$ identically track the corresponding corrections in the HTL, while the nominal predictions substantially diverge.

Next, in figure 6 we turn to the phenomenologically important dijet invariant mass distribution. Again we consider an inclusive selection (left) and a boosted selection requiring $p_{T,H} > 300\,\mathrm{GeV}$. In the inclusive phase-space the NLO corrections are about 50% in the $\mathrm{FT}_{\mathrm{approx}}$ with hardly any variations over the considered $m_{j_1 j_2}$ range. Corrections in the HTL are identical to the $\mathrm{FT}_{\mathrm{approx}}$ at small $m_{j_1 j_2}$ and slightly reduce to about 40% in the multi TeV range, i.e. up to 10% smaller than in the $\mathrm{FT}_{\mathrm{approx}}$. With the boosted selection, corrections in both the $\mathrm{FT}_{\mathrm{approx}}$ and the HTL are at the level of 30–40% and marginally reduce in the tail of the $m_{j_1 j_2}$ distribution.

Finally in figure 7 we plot the rapidity difference between the two jets in H + 2 jets production, again with an inclusive selection on the left and a boosted selection on the right. In the inclusive case there is hardly any variation in the NLO corrections over the considered rapidity range with a K-factor at the 1.5 level. For the boosted selection, the K-factor decreases slightly from about 1.35 to 1.25 from small to high rapidity differences. For both selections and over the entire rapidity range corrections in the $\mathrm{FT}_{\mathrm{approx}}$ and the
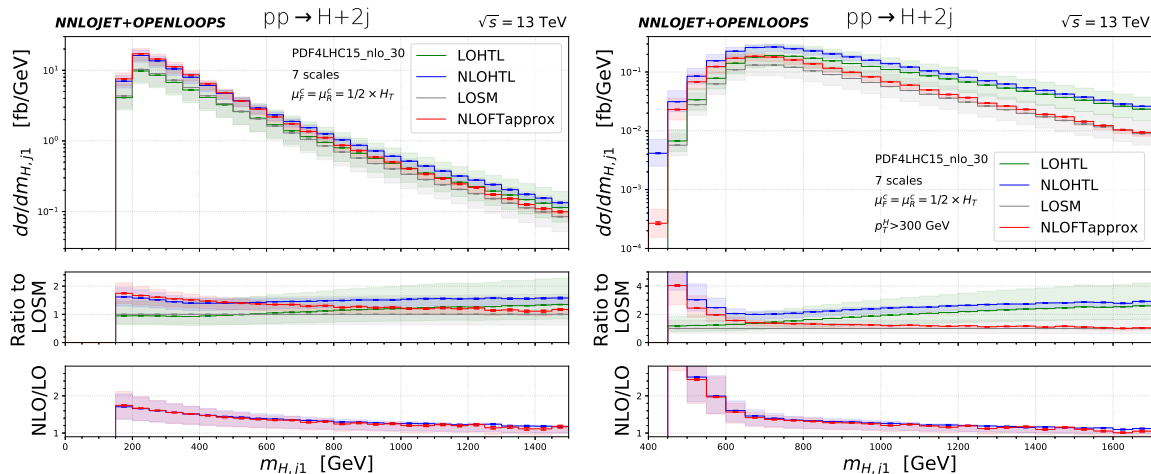
Figure 5. Invariant mass distribution of the Higgs and the hardest jet system in H+2 jets production. Colour coding and labelling as in figure 2.
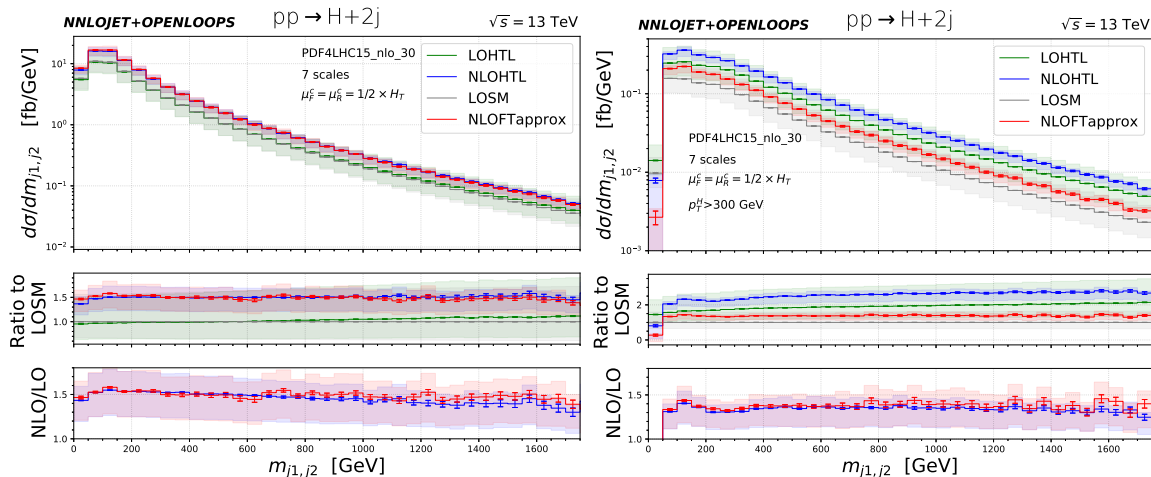

Figure 6. Invariant mass distribution of the di-jet system in H + 2 jets production. Colour coding and labelling as in figure 2.

HTL agree at the percent level. We observed very similar findings also in other angular correlation observables including e.g. the rapidity difference between the Higgs and the hardest jet.

Overall in all considered observables we find a remarkable agreement of the relative corrections computed in the HTL and the FT_{approx} — despite up to several order of magnitude variations in nominal predictions. This clearly points towards a factorisation of QCD higher-order corrections from the heavy fermion loop mediating the coupling of the Higgs boson.
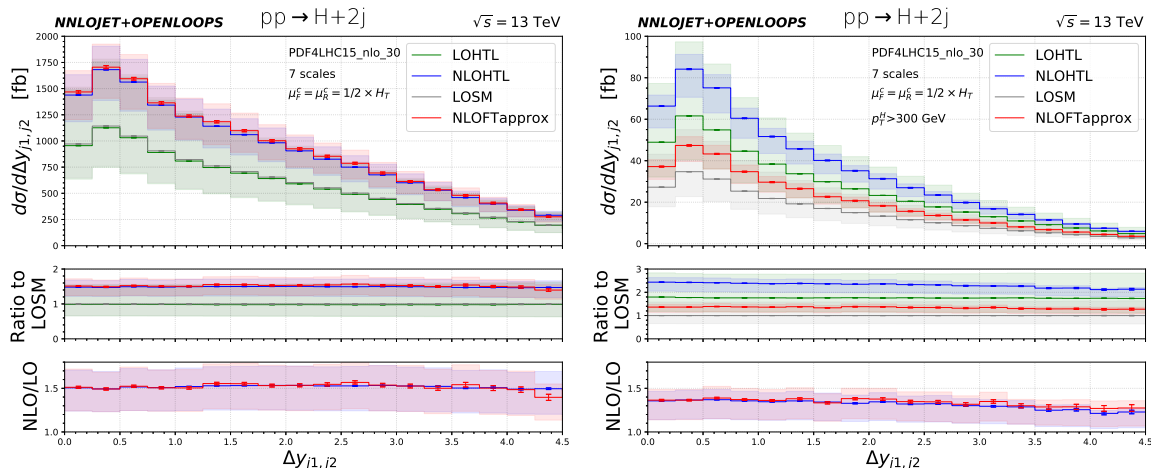
Figure 7. Rapidity difference between the two hardest jets in H + 2 jets production. Colour coding and labelling as in figure 2.

4 Conclusions

In this paper we have presented precise differential predictions for H+jet and H + 2 jets production at the LHC at NLO including top-quark mass effects. For the former process our prediction incorporates the exact top-quark mass dependence. Instead, in our study of H + 2 jets production, the two-loop virtual matrix elements are computed in the HTL approximation (infinite top-quark mass) and reweighed by the full LO result, while the exact top-quark mass dependence is retained in the Born and real radiation contributions. Our results are produced using the NNLOJET event generator with one-loop amplitudes provided by OPENLOOPS2.2 (to be released soon) which implements a novel tensor reduction method based on the on-the-fly reduction algorithm of OpenLoops. The two-loop virtual matrix elements including top-quark mass effects contributing to H+jet production are evaluated using SECDEC-3.

We find that the inclusion of the exact top-quark mass dependence in the two-loop virtual matrix elements enhances the cross section for H+jet production at NLO by about 0.6% with respect to the FT_{approx} prediction, and by about 4.3% with respect to the HTL prediction. However, the NLO/LO K-factor is found to be universal amongst the three predictions at about 1.7. Noteworthy, this universality is broadly also found examining the corrections to the $p_{T,H}$ and $p_{T,j}$ distributions. Although above the top-quark threshold the HTL approximation becomes formally invalid, relative NLO corrections agree at the 10% (5%) level between HTL (FT_{approx}) respectively and the full theory.

Regarding the H + 2 jets production process we have produced distributions for the p_T of the Higgs boson and leading jet as well as invariant mass distributions for the Higgs + leading jet system and the leading dijet system. In particular the latter is crucial for gluon-fusion Higgs production backgrounds in VBF Higgs production analyses. At the inclusive level the FT_{approx} cross section is 2.8% larger than the HTL prediction. Differentially, we observe that the approximate inclusion of the top-quark mass has the largest, though still rather

mild, impact on the p_T distributions above the top-quark threshold. Relative higher-order corrections in the HTL and the FT_{approx} always agree at below the 10% level.

Overall, the top-quark mass effects at NLO are observed to be rather mild. In particular they are expected to be at the same level or even smaller than the current uncertainties due to the scheme dependence of the top-quark mass.

The computations presented are relevant for analyses of Higgs production at large transverse momentum and also for Higgs plus multi-jet backgrounds in Higgs production via vector boson fusion. Through detailed comparisons, this study proves the reliability of higher-order corrections computed in the HTL rescaled with lower-order predictions with explicit mass dependence. The multiplicative reweighting procedures are of similar theoretical uncertainties, within 10%, for both event-by-event and bin-by-bin rescaling. This paves the way towards computations of $pp \to H + j$ including approximate mass effects at NNLO and higher QCD accuracy.

Acknowledgments

A Inclusive cross sections

In table 3 and table 4 we list as reference integrated cross sections $\sigma(p_{T,H} > p_{T,H}^{\text{cut}})$ in function of $p_{T,H}^{\text{cut}}$ for $pp \to H + j$ and $pp \to H + jj$ respectively. Shown are cross sections at LO and NLO and related K-factors considering the HTL and FT$_{\text{approx}}$ approximations, and for $pp \to H + j$ also the results with exact top-mass dependence. The setup is given in section 3.1.

$p_{T,H}^{\text{cut}}$	LO$_{\text{HTL}}$	NLO$_{\text{HTL}}$	K$_{\text{HTL}}^{\text{NLO}}$	LO$_{\text{SM}}$	NLO$_{\text{FT}_{\text{approx}}}$	K$_{\text{FT}_{\text{approx}}}^{\text{NLO}}$	NLO$_{\text{SM}}$	K$_{\text{SM}}^{\text{NLO}}$
50	4453^{+1755}_{-1181}	8482^{+1755}_{-1522}	1.90	4566^{+1800}_{-1212}	8682^{+1793}_{-1557}	1.90	8732^{+1858}_{-1585}	1.91
100	1430^{+585}_{-389}	2732^{+578}_{-502}	1.91	1391^{+570}_{-379}	2645^{+557}_{-485}	1.90	2669^{+575}_{-494}	1.92
150	593^{+249}_{-164}	1121^{+235}_{-207}	1.89	528^{+222}_{-146}	989^{+205}_{-182}	1.87	996^{+216}_{-186}	1.89
200	$284^{+121}_{-79.6}$	$533^{+111}_{-98.9}$	1.88	$219^{+94.2}_{-61.7}$	$411^{+85.9}_{-76.5}$	1.88	$417^{+90.0}_{-78.4}$	1.90
250	$151^{+65.2}_{-42.6}$	$281^{+58.2}_{-52.2}$	1.87	$97.4^{+42.5}_{-27.7}$	$184^{+39.3}_{-34.8}$	1.89	$189^{+41.2}_{-36.1}$	1.94
300	$85.9^{+37.6}_{-24.5}$	$160^{+32.9}_{-29.7}$	1.86	$45.9^{+20.3}_{-13.2}$	$87.8^{+19.2}_{-16.9}$	1.91	$90.1^{+19.7}_{-17.4}$	1.96
350	$51.8^{+22.9}_{-14.8}$	$95.9^{+19.7}_{-17.9}$	1.85	$22.9^{+10.2}_{-6.62}$	$44.0^{+9.71}_{-8.53}$	1.92	$45.1^{+10.2}_{-8.85}$	1.97
400	$32.5^{+14.5}_{-9.38}$	$60.1^{+12.3}_{-11.2}$	1.85	$12.0^{+5.39}_{-3.48}$	$23.0^{+5.10}_{-4.49}$	1.92	$23.6^{+5.38}_{-4.66}$	1.98
450	$21.2^{+9.49}_{-6.14}$	$39.1^{+8.00}_{-7.33}$	1.84	$6.52^{+2.96}_{-1.91}$	$12.6^{+2.80}_{-2.46}$	1.93	$12.9^{+2.97}_{-2.56}$	1.98
500	$14.2^{+6.39}_{-4.13}$	$26.2^{+5.36}_{-4.92}$	1.84	$3.67^{+1.68}_{-1.08}$	$7.09^{+1.59}_{-1.40}$	1.93	$7.25^{+1.69}_{-1.45}$	1.97
550	$9.71^{+4.40}_{-2.84}$	$17.9^{+3.66}_{-3.37}$	1.84	$2.14^{+0.98}_{-0.63}$	$4.11^{+0.92}_{-0.81}$	1.92	$4.18^{+0.96}_{-0.83}$	1.96
600	$6.79^{+3.09}_{-1.99}$	$12.5^{+2.56}_{-2.36}$	1.84	$1.28^{+0.59}_{-0.38}$	$2.47^{+0.56}_{-0.49}$	1.93	$2.50^{+0.59}_{-0.51}$	1.96
650	$4.82^{+2.21}_{-1.42}$	$8.88^{+1.83}_{-1.69}$	1.84	$0.78^{+0.36}_{-0.23}$	$1.50^{+0.34}_{-0.30}$	1.92	$1.53^{+0.36}_{-0.31}$	1.96
700	$3.48^{+1.60}_{-1.03}$	$6.42^{+1.33}_{-1.22}$	1.85	$0.49^{+0.23}_{-0.15}$	$0.94^{+0.21}_{-0.19}$	1.92	$0.96^{+0.23}_{-0.19}$	1.96
750	$2.54^{+1.17}_{-0.75}$	$4.68^{+0.97}_{-0.89}$	1.84	$0.31^{+0.15}_{-0.09}$	$0.60^{+0.14}_{-0.12}$	1.94	$0.62^{+0.14}_{-0.13}$	1.97
800	$1.87^{+0.87}_{-0.56}$	$3.45^{+0.71}_{-0.66}$	1.84	$0.20^{+0.1}_{-0.06}$	$0.39^{+0.09}_{-0.08}$	1.92	$0.39^{+0.09}_{-0.08}$	1.94

Table 3. Integrated cross sections in fb depending on $p_{T,H}^{\text{cut}}$ at LO and NLO in the HTL, FT$_{\text{approx}}$, and with full top-quark mass dependence (SM) for H+jet production at the LHC with $\sqrt{S} = 13\,\text{TeV}$ together with corresponding K-factors. Uncertainties correspond to the envelope of 7-point scale variations. We require $p_{\text{T,j}} > 30\,\text{GeV}$.

$p_{T,H}^{\mathrm{cut}}$	$\mathrm{LO_{HTL}}$	$\mathrm{NLO_{HTL}}$	$\mathrm{K_{HTL}^{NLO}}$	$\mathrm{LO_{SM}}$	$\mathrm{NLO_{FT_{approx}}}$	$\mathrm{K_{FT_{approx}}^{NLO}}$
50	2365^{+1377}_{-813}	3511^{+446}_{-631}	1.48	2387^{+1391}_{-821}	3574^{+477}_{-651}	1.50
100	1355^{+790}_{-466}	2025^{+267}_{-368}	1.50	1317^{+769}_{-454}	1991^{+276}_{-368}	1.51
150	671^{+392}_{-232}	969^{+110}_{-169}	1.44	601^{+353}_{-208}	881^{+107}_{-157}	1.47
200	355^{+208}_{-123}	$497^{+47.9}_{-83.4}$	1.40	$281^{+166}_{-97.5}$	$399^{+42.1}_{-68.7}$	1.42
250	$201^{+118}_{-69.6}$	$274^{+22.7}_{-44.4}$	1.36	$136^{+80.2}_{-47.2}$	$188^{+17.8}_{-31.6}$	1.39
300	$120^{+70.5}_{-41.6}$	$160^{+11.8}_{-25.3}$	1.34	$68.1^{+40.3}_{-23.7}$	$92.4^{+7.73}_{-15.2}$	1.36
350	$74.8^{+44.0}_{-26.0}$	$98.5^{+6.53}_{-15.2}$	1.32	$35.5^{+21.1}_{-12.4}$	$47.7^{+3.70}_{-7.73}$	1.34
400	$48.4^{+28.5}_{-16.8}$	$62.9^{+3.82}_{-9.56}$	1.30	$19.2^{+11.4}_{-6.71}$	$25.4^{+1.82}_{-4.05}$	1.33
450	$32.2^{+19.0}_{-11.2}$	$41.5^{+2.36}_{-6.23}$	1.29	$10.7^{+6.38}_{-3.75}$	$14.1^{+0.96}_{-2.23}$	1.32
500	$21.9^{+12.9}_{-7.62}$	$28.0^{+1.51}_{-4.18}$	1.28	$6.16^{+3.68}_{-2.16}$	$8.06^{+0.52}_{-1.27}$	1.31
550	$15.2^{+8.99}_{-5.30}$	$19.4^{+1.01}_{-2.87}$	1.27	$3.64^{+2.18}_{-1.28}$	$4.74^{+0.30}_{-0.74}$	1.30
600	$10.8^{+6.37}_{-3.75}$	$13.7^{+0.69}_{-2.02}$	1.27	$2.20^{+1.32}_{-0.77}$	$2.85^{+0.18}_{-0.44}$	1.29
650	$7.72^{+4.57}_{-2.70}$	$9.79^{+0.49}_{-1.44}$	1.27	$1.36^{+0.82}_{-0.48}$	$1.76^{+0.11}_{-0.27}$	1.29
700	$5.61^{+3.33}_{-1.96}$	$7.10^{+0.35}_{-1.05}$	1.27	$0.85^{+0.51}_{-0.30}$	$1.10^{+0.07}_{-0.17}$	1.29
750	$4.12^{+2.45}_{-1.44}$	$5.22^{+0.25}_{-0.77}$	1.26	$0.55^{+0.33}_{-0.19}$	$0.70^{+0.04}_{-0.11}$	1.29
800	$3.06^{+1.82}_{-1.07}$	$3.88^{+0.19}_{-0.57}$	1.27	$0.36^{+0.22}_{-0.13}$	$0.46^{+0.03}_{-0.07}$	1.28

Table 4. Integrated cross sections in fb depending on $p_{T,H}^{\mathrm{cut}}$ at LO and NLO in the HTL and $\mathrm{FT_{approx}}$ for H + 2 jets production at the LHC with $\sqrt{S} = 13\,\mathrm{TeV}$ together with corresponding K-factors. Uncertainties correspond to the envelope of 7-point scale variations. We require $p_{T,j_1} > 40\,\mathrm{GeV}$, $p_{T,j_2} > 30\,\mathrm{GeV}$.

References

[1] C. Arnesen, I.Z. Rothstein and J. Zupan, *Smoking Guns for On-Shell New Physics at the LHC*, *Phys. Rev. Lett.* **103** (2009) 151801 [arXiv:0809.1429] [INSPIRE].

[2] A. Banfi, A. Martin and V. Sanz, *Probing top-partners in Higgs+jets*, *JHEP* **08** (2014) 053 [arXiv:1308.4771] [INSPIRE].

[3] A. Azatov and A. Paul, *Probing Higgs couplings with high p_T Higgs production*, *JHEP* **01** (2014) 014 [arXiv:1309.5273] [INSPIRE].

[4] C. Grojean, E. Salvioni, M. Schlaffer and A. Weiler, *Very boosted Higgs in gluon fusion*, *JHEP* **05** (2014) 022 [arXiv:1312.3317] [INSPIRE].

[5] R.V. Harlander and T. Neumann, *Probing the nature of the Higgs-gluon coupling*, *Phys. Rev. D* **88** (2013) 074015 [arXiv:1308.2225] [INSPIRE].

[6] S. Dawson, I.M. Lewis and M. Zeng, *Effective field theory for Higgs boson plus jet production*, *Phys. Rev. D* **90** (2014) 093007 [arXiv:1409.6299] [INSPIRE].

[7] U. Langenegger, M. Spira and I. Strebel, *Testing the Higgs Boson Coupling to Gluons*, arXiv:1507.01373 [INSPIRE].

[8] M. Grazzini, A. Ilnicka, M. Spira and M. Wiesemann, *Modeling BSM effects on the Higgs transverse-momentum spectrum in an EFT approach*, *JHEP* **03** (2017) 115 [arXiv:1612.00283] [INSPIRE].

[9] N. Deutschmann, C. Duhr, F. Maltoni and E. Vryonidou, *Gluon-fusion Higgs production in the Standard Model Effective Field Theory*, *JHEP* **12** (2017) 063 [*Erratum ibid.* **02** (2018) 159] [arXiv:1708.00460] [INSPIRE].

[10] M. Battaglia, M. Grazzini, M. Spira and M. Wiesemann, *Sensitivity to BSM effects in the Higgs p_T spectrum within SMEFT*, *JHEP* **11** (2021) 173 [arXiv:2109.02987] [INSPIRE].

[11] ATLAS collaboration, *Prospects for differential cross-section measurements of Higgs boson production measured in decays to ZZ and $\gamma\gamma$ with the ATLAS experiment at the High-Luminosity LHC*, ATL-PHYS-PUB-2018-040 (2018).

[12] CMS collaboration, *Sensitivity projections for Higgs boson properties measurements at the HL-LHC*, CMS-PAS-FTR-18-011 (2018).

[13] ATLAS collaboration, *Study of Higgs-boson production with large transverse momentum using the $H \to b\bar{b}$ decay with the ATLAS detector*, ATLAS-CONF-2021-010 (2021).

[14] CMS collaboration, *Inclusive search for highly boosted Higgs bosons decaying to bottom quark-antiquark pairs in proton-proton collisions at $\sqrt{s} = 13\,TeV$*, *JHEP* **12** (2020) 085 [arXiv:2006.13251] [INSPIRE].

[15] K. Becker et al., *Precise predictions for boosted Higgs production*, arXiv:2005.07762 [INSPIRE].

[16] F. Campanario, T.M. Figy, S. Plätzer, M. Rauch, P. Schichtel and M. Sjödahl, *Stress testing the vector-boson-fusion approximation in multijet final states*, *Phys. Rev. D* **98** (2018) 033003 [arXiv:1802.09955] [INSPIRE].

[17] A. Buckley et al., *A comparative study of Higgs boson production from vector-boson fusion*, *JHEP* **11** (2021) 108 [arXiv:2105.11399] [INSPIRE].

[18] P. Artoisenet et al., *A framework for Higgs characterisation*, *JHEP* **11** (2013) 043 [arXiv:1306.6464] [INSPIRE].

[19] F. Maltoni, K. Mawatari and M. Zaro, *Higgs characterisation via vector-boson fusion and associated production: NLO and parton-shower effects*, *Eur. Phys. J. C* **74** (2014) 2710 [arXiv:1311.1829] [INSPIRE].

[20] A. Greljo, G. Isidori, J.M. Lindert and D. Marzocca, *Pseudo-observables in electroweak Higgs production*, *Eur. Phys. J. C* **76** (2016) 158 [arXiv:1512.06135] [INSPIRE].

[21] C. Degrande, B. Fuks, K. Mawatari, K. Mimasu and V. Sanz, *Electroweak Higgs boson production in the standard model effective field theory beyond leading order in QCD*, *Eur. Phys. J. C* **77** (2017) 262 [arXiv:1609.04833] [INSPIRE].

[22] A. Greljo, G. Isidori, J.M. Lindert, D. Marzocca and H. Zhang, *Electroweak Higgs production with HiggsPO at NLO QCD*, *Eur. Phys. J. C* **77** (2017) 838 [arXiv:1710.04143] [INSPIRE].

[23] J.Y. Araz, S. Banerjee, R.S. Gupta and M. Spannowsky, *Precision SMEFT bounds from the VBF Higgs at high transverse momentum*, *JHEP* **04** (2021) 125 [arXiv:2011.03555] [INSPIRE].

[24] M. Czakon, R.V. Harlander, J. Klappert and M. Niggetiedt, *Exact Top-Quark Mass Dependence in Hadronic Higgs Production*, *Phys. Rev. Lett.* **127** (2021) 162002 [arXiv:2105.04436] [INSPIRE].

[25] S.P. Jones, M. Kerner and G. Luisoni, *Next-to-Leading-Order QCD Corrections to Higgs Boson Plus Jet Production with Full Top-Quark Mass Dependence*, *Phys. Rev. Lett.* **120** (2018) 162001 [arXiv:1802.00349] [*Erratum ibid.* **128** (2022) 059901] [INSPIRE].

[26] J.M. Lindert, K. Kudashkin, K. Melnikov and C. Wever, *Higgs bosons with large transverse momentum at the LHC*, *Phys. Lett. B* **782** (2018) 210 [arXiv:1801.08226] [INSPIRE].

[27] T. Neumann, *NLO Higgs+jet production at large transverse momenta including top quark mass effects*, *J. Phys. Comm.* **2** (2018) 095017 [arXiv:1802.02981] [INSPIRE].

[28] M. Kerner, *Top mass effects in HJ and HH production*, *PoS* **RADCOR2019** (2019) 020 [INSPIRE].

[29] V. Del Duca, W. Kilgore, C. Oleari, C. Schmidt and D. Zeppenfeld, *Higgs + 2 jets via gluon fusion*, *Phys. Rev. Lett.* **87** (2001) 122001 [hep-ph/0105129] [INSPIRE].

[30] V. Del Duca, W. Kilgore, C. Oleari, C. Schmidt and D. Zeppenfeld, *Gluon fusion contributions to H + 2 jet production*, *Nucl. Phys. B* **616** (2001) 367 [hep-ph/0108030] [INSPIRE].

[31] T. Neumann and C. Williams, *The Higgs boson at high p_T*, *Phys. Rev. D* **95** (2017) 014004 [arXiv:1609.00367] [INSPIRE].

[32] J.R. Andersen, J.D. Cockburn, M. Heil, A. Maier and J.M. Smillie, *Finite Quark-Mass Effects in Higgs Boson Production with Dijets at Large Energies*, *JHEP* **04** (2019) 127 [arXiv:1812.08072] [INSPIRE].

[33] L. Budge, J.M. Campbell, G. De Laurentis, R.K. Ellis and S. Seth, *The one-loop amplitudes for Higgs + 4 partons with full mass effects*, *JHEP* **05** (2020) 079 [arXiv:2002.04018] [INSPIRE].

[34] R. Frederix, S. Frixione, E. Vryonidou and M. Wiesemann, *Heavy-quark mass effects in Higgs plus jets production*, *JHEP* **08** (2016) 006 [arXiv:1604.03017] [INSPIRE].

[35] S. Borowka, G. Heinrich, S.P. Jones, M. Kerner, J. Schlenk and T. Zirke, *SecDec-3.0: numerical evaluation of multi-scale integrals beyond one loop*, *Comput. Phys. Commun.* **196** (2015) 470 [arXiv:1502.06595] [INSPIRE].

[36] S. Borowka et al., *pySecDec: a toolbox for the numerical evaluation of multi-scale integrals*, *Comput. Phys. Commun.* **222** (2018) 313 [arXiv:1703.09692] [INSPIRE].

[37] K. Kudashkin, K. Melnikov and C. Wever, *Two-loop amplitudes for processes $gg \to Hg, qg \to Hq$ and $q\bar{q} \to Hg$ at large Higgs transverse momentum*, *JHEP* **02** (2018) 135 [arXiv:1712.06549] [INSPIRE].

[38] F. Wilczek, *Decays of Heavy Vector Mesons Into Higgs Particles*, *Phys. Rev. Lett.* **39** (1977) 1304 [INSPIRE].

[39] C. Anastasiou, C. Duhr, F. Dulat, F. Herzog and B. Mistlberger, *Higgs Boson Gluon-Fusion Production in QCD at Three Loops*, *Phys. Rev. Lett.* **114** (2015) 212001 [arXiv:1503.06056] [INSPIRE].

[40] F. Dulat, B. Mistlberger and A. Pelloni, *Differential Higgs production at N^3LO beyond threshold*, *JHEP* **01** (2018) 145 [arXiv:1710.03016] [INSPIRE].

[41] L. Cieri, X. Chen, T. Gehrmann, E.W.N. Glover and A. Huss, *Higgs boson production at the LHC using the q_T subtraction formalism at N^3LO QCD*, *JHEP* **02** (2019) 096 [arXiv:1807.11501] [INSPIRE].

[42] B. Mistlberger, *Higgs boson production at hadron colliders at N^3LO in QCD*, *JHEP* **05** (2018) 028 [arXiv:1802.00833] [INSPIRE].

[43] X. Chen, T. Gehrmann, E.W.N. Glover, A. Huss, B. Mistlberger and A. Pelloni, *Fully Differential Higgs Boson Production to Third Order in QCD*, *Phys. Rev. Lett.* **127** (2021) 072002 [arXiv:2102.07607] [INSPIRE].

[44] G. Billis, B. Dehnadi, M.A. Ebert, J.K.L. Michel and F.J. Tackmann, *Higgs pT Spectrum and Total Cross Section with Fiducial Cuts at Third Resummed and Fixed Order in QCD*, *Phys. Rev. Lett.* **127** (2021) 072001 [arXiv:2102.08039] [INSPIRE].

[45] R. Boughezal, F. Caola, K. Melnikov, F. Petriello and M. Schulze, *Higgs boson production in association with a jet at next-to-next-to-leading order in perturbative QCD*, *JHEP* **06** (2013) 072 [arXiv:1302.6216] [INSPIRE].

[46] X. Chen, T. Gehrmann, E.W.N. Glover and M. Jaquier, *Precise QCD predictions for the production of Higgs + jet final states*, *Phys. Lett. B* **740** (2015) 147 [arXiv:1408.5325] [INSPIRE].

[47] R. Boughezal, F. Caola, K. Melnikov, F. Petriello and M. Schulze, *Higgs boson production in association with a jet at next-to-next-to-leading order*, *Phys. Rev. Lett.* **115** (2015) 082003 [arXiv:1504.07922] [INSPIRE].

[48] R. Boughezal, C. Focke, W. Giele, X. Liu and F. Petriello, *Higgs boson production in association with a jet at NNLO using jettiness subtraction*, *Phys. Lett. B* **748** (2015) 5 [arXiv:1505.03893] [INSPIRE].

[49] X. Chen, J. Cruz-Martinez, T. Gehrmann, E.W.N. Glover and M. Jaquier, *NNLO QCD corrections to Higgs boson production at large transverse momentum*, *JHEP* **10** (2016) 066 [arXiv:1607.08817] [INSPIRE].

[50] J.M. Campbell, R.K. Ellis and G. Zanderighi, *Next-to-Leading order Higgs + 2 jet production via gluon fusion*, *JHEP* **10** (2006) 028 [hep-ph/0608194] [INSPIRE].

[51] H. van Deurzen et al., *NLO QCD corrections to the production of Higgs plus two jets at the LHC*, *Phys. Lett. B* **721** (2013) 74 [arXiv:1301.0493] [INSPIRE].

[52] G. Cullen et al., *Next-to-Leading-Order QCD Corrections to Higgs Boson Production Plus Three Jets in Gluon Fusion*, *Phys. Rev. Lett.* **111** (2013) 131801 [arXiv:1307.4737] [INSPIRE].

[53] G. Bozzi, S. Catani, D. de Florian and M. Grazzini, *Transverse-momentum resummation and the spectrum of the Higgs boson at the LHC*, *Nucl. Phys. B* **737** (2006) 73 [hep-ph/0508068] [INSPIRE].

[54] D. de Florian, G. Ferrera, M. Grazzini and D. Tommasini, *Transverse-momentum resummation: Higgs boson production at the Tevatron and the LHC*, *JHEP* **11** (2011) 064 [arXiv:1109.2109] [INSPIRE].

[55] T. Becher, M. Neubert and D. Wilhelm, *Higgs-Boson Production at Small Transverse Momentum*, *JHEP* **05** (2013) 110 [arXiv:1212.2621] [INSPIRE].

[56] W. Bizon, P.F. Monni, E. Re, L. Rottoli and P. Torrielli, *Momentum-space resummation for transverse observables and the Higgs $p_\perp$ at $N^3LL + NNLO$*, *JHEP* **02** (2018) 108 [arXiv:1705.09127] [INSPIRE].

[57] X. Chen et al., *Precise QCD Description of the Higgs Boson Transverse Momentum Spectrum*, *Phys. Lett. B* **788** (2019) 425 [arXiv:1805.00736] [INSPIRE].

[58] W. Bizoń et al., *Fiducial distributions in Higgs and Drell-Yan production at $N^3LL + NNLO$*, *JHEP* **12** (2018) 132 [arXiv:1805.05916] [INSPIRE].

[59] E. Re, L. Rottoli and P. Torrielli, *Fiducial Higgs and Drell-Yan distributions at $N^3LL' + NNLO$ with RadISH*, arXiv:2104.07509 [INSPIRE].

[60] H. Mantler and M. Wiesemann, *Top- and bottom-mass effects in hadronic Higgs production at small transverse momenta through $LO + NLL$*, *Eur. Phys. J. C* **73** (2013) 2467 [arXiv:1210.8263] [INSPIRE].

[61] M. Grazzini and H. Sargsyan, *Heavy-quark mass effects in Higgs boson production at the LHC*, *JHEP* **09** (2013) 129 [arXiv:1306.4581] [INSPIRE].

[62] A. Banfi, P.F. Monni and G. Zanderighi, *Quark masses in Higgs production with a jet veto*, *JHEP* **01** (2014) 097 [arXiv:1308.4634] [INSPIRE].

[63] K. Melnikov, L. Tancredi and C. Wever, *Two-loop $gg \to Hg$ amplitude mediated by a nearly massless quark*, *JHEP* **11** (2016) 104 [arXiv:1610.03747] [INSPIRE].

[64] J.M. Lindert, K. Melnikov, L. Tancredi and C. Wever, *Top-bottom interference effects in Higgs plus jet production at the LHC*, *Phys. Rev. Lett.* **118** (2017) 252002 [arXiv:1703.03886] [INSPIRE].

[65] K. Melnikov, L. Tancredi and C. Wever, *Two-loop amplitudes for $qg \to Hq$ and $q\bar{q} \to Hg$ mediated by a nearly massless quark*, *Phys. Rev. D* **95** (2017) 054012 [arXiv:1702.00426] [INSPIRE].

[66] F. Caola, J.M. Lindert, K. Melnikov, P.F. Monni, L. Tancredi and C. Wever, *Bottom-quark effects in Higgs production at intermediate transverse momentum*, *JHEP* **09** (2018) 035 [arXiv:1804.07632] [INSPIRE].

[67] F. Caola, S. Forte, S. Marzani, C. Muselli and G. Vita, *The Higgs transverse momentum spectrum with finite quark masses beyond leading order*, *JHEP* **08** (2016) 150 [arXiv:1606.04100] [INSPIRE].

[68] R.V. Harlander, T. Neumann, K.J. Ozeren and M. Wiesemann, *Top-mass effects in differential Higgs production through gluon fusion at order* $\mathcal{O}(\alpha_s^4)$, *JHEP* **08** (2012) 139 [arXiv:1206.0157] [INSPIRE].

[69] T. Neumann and M. Wiesemann, *Finite top-mass effects in gluon-induced Higgs production with a jet-veto at NNLO*, *JHEP* **11** (2014) 150 [arXiv:1408.6836] [INSPIRE].

[70] J.M. Campbell, R.K. Ellis, R. Frederix, P. Nason, C. Oleari and C. Williams, *NLO Higgs Boson Production Plus One and Two Jets Using the POWHEG BOX, MadGraph4 and MCFM*, *JHEP* **07** (2012) 092 [arXiv:1202.5475] [INSPIRE].

[71] K. Hamilton, P. Nason, C. Oleari and G. Zanderighi, *Merging H/W/Z + 0 and 1 jet at NLO with no merging scale: a path to parton shower + NNLO matching*, *JHEP* **05** (2013) 082 [arXiv:1212.4504] [INSPIRE].

[72] M. Buschmann, D. Goncalves, S. Kuttimalai, M. Schonherr, F. Krauss and T. Plehn, *Mass Effects in the Higgs-Gluon Coupling: Boosted vs Off-Shell Production*, *JHEP* **02** (2015) 038 [arXiv:1410.5806] [INSPIRE].

[73] N. Greiner, S. Höche, G. Luisoni, M. Schönherr and J.-C. Winter, *Full mass dependence in Higgs boson production in association with jets at the LHC and FCC*, *JHEP* **01** (2017) 091 [arXiv:1608.01195] [INSPIRE].

[74] F. Maltoni, E. Vryonidou and M. Zaro, *Top-quark mass effects in double and triple Higgs production in gluon-gluon fusion at NLO*, *JHEP* **11** (2014) 079 [arXiv:1408.6542] [INSPIRE].

[75] A. Gehrmann-De Ridder, T. Gehrmann and E.W.N. Glover, *Antenna subtraction at NNLO*, *JHEP* **09** (2005) 056 [hep-ph/0505111] [INSPIRE].

[76] A. Gehrmann-De Ridder, T. Gehrmann and E.W.N. Glover, *Gluon-gluon antenna functions from Higgs boson decay*, *Phys. Lett. B* **612** (2005) 49 [hep-ph/0502110] [INSPIRE].

[77] A. Daleo, T. Gehrmann and D. Maître, *Antenna subtraction with hadronic initial states*, *JHEP* **04** (2007) 016 [hep-ph/0612257] [INSPIRE].

[78] A. Daleo, A. Gehrmann-De Ridder, T. Gehrmann and G. Luisoni, *Antenna subtraction at NNLO with hadronic initial states: initial-final configurations*, *JHEP* **01** (2010) 118 [arXiv:0912.0374] [INSPIRE].

[79] E.W. Nigel Glover and J. Pires, *Antenna subtraction for gluon scattering at NNLO*, *JHEP* **06** (2010) 096 [arXiv:1003.2824] [INSPIRE].

[80] A. Gehrmann-De Ridder, E.W.N. Glover and J. Pires, *Real-Virtual corrections for gluon scattering at NNLO*, *JHEP* **02** (2012) 141 [arXiv:1112.3613] [INSPIRE].

[81] A. Gehrmann-De Ridder, T. Gehrmann and M. Ritzmann, *Antenna subtraction at NNLO with hadronic initial states: double real initial-initial configurations*, *JHEP* **10** (2012) 047 [arXiv:1207.5779] [INSPIRE].

[82] A. Gehrmann-De Ridder, T. Gehrmann, E.W.N. Glover and J. Pires, *Double Virtual corrections for gluon scattering at NNLO*, *JHEP* **02** (2013) 026 [arXiv:1211.2710] [INSPIRE].

[83] J. Currie, E.W.N. Glover and S. Wells, *Infrared Structure at NNLO Using Antenna Subtraction*, *JHEP* **04** (2013) 066 [arXiv:1301.4693] [INSPIRE].

[84] F. Cascioli, P. Maierhofer and S. Pozzorini, *Scattering Amplitudes with Open Loops*, *Phys. Rev. Lett.* **108** (2012) 111601 [arXiv:1111.5206] [INSPIRE].

[85] F. Buccioni, S. Pozzorini and M. Zoller, *On-the-fly reduction of open loops*, *Eur. Phys. J. C* **78** (2018) 70 [arXiv:1710.11452] [INSPIRE].

[86] F. Buccioni et al., *OpenLoops 2*, *Eur. Phys. J. C* **79** (2019) 866 [arXiv:1907.13071] [INSPIRE].

[87] J.-N. Lang et al, *OTTER: On-The-fly Tensor Reduction*, in preparation.

[88] R. Frederix et al., *Higgs pair production at the LHC with NLO and parton-shower effects*, *Phys. Lett. B* **732** (2014) 142 [arXiv:1401.7340] [INSPIRE].

[89] S. Catani, *The Singular behavior of QCD amplitudes at two loop order*, *Phys. Lett. B* **427** (1998) 161 [hep-ph/9802439] [INSPIRE].

[90] M. Grazzini et al., *Higgs boson pair production at NNLO with top quark mass effects*, *JHEP* **05** (2018) 059 [arXiv:1803.02463] [INSPIRE].

[91] A. Denner, S. Dittmaier and L. Hofer, *Collier: a fortran-based Complex One-Loop LIbrary in Extended Regularizations*, *Comput. Phys. Commun.* **212** (2017) 220 [arXiv:1604.06792] [INSPIRE].

[92] A. van Hameren, *OneLOop: For the evaluation of one-loop scalar functions*, *Comput. Phys. Commun.* **182** (2011) 2427 [arXiv:1007.4716] [INSPIRE].

[93] A. von Manteuffel and C. Studerus, *Reduze 2 — Distributed Feynman Integral Reduction*, arXiv:1201.4330 [INSPIRE].

[94] Z. Li, J. Wang, Q.-S. Yan and X. Zhao, *Efficient numerical evaluation of Feynman integrals*, *Chin. Phys. C* **40** (2016) 033103 [arXiv:1508.02512] [INSPIRE].

[95] S. Borowka, G. Heinrich, S. Jahn, S.P. Jones, M. Kerner and J. Schlenk, *A GPU compatible quasi-Monte Carlo integrator interfaced to pySecDec*, *Comput. Phys. Commun.* **240** (2019) 120 [arXiv:1811.11720] [INSPIRE].

[96] J. Baglio, F. Campanario, S. Glaus, M. Mühlleitner, M. Spira and J. Streicher, *Gluon fusion into Higgs pairs at NLO QCD and the top mass scheme*, *Eur. Phys. J. C* **79** (2019) 459 [arXiv:1811.05692] [INSPIRE].

[97] J. Baglio et al., *Higgs-Pair Production via Gluon Fusion at Hadron Colliders: NLO QCD Corrections*, *JHEP* **04** (2020) 181 [arXiv:2003.03227] [INSPIRE].

[98] J. Baglio, F. Campanario, S. Glaus, M. Mühlleitner, J. Ronca and M. Spira, *gg → HH: Combined uncertainties*, *Phys. Rev. D* **103** (2021) 056002 [arXiv:2008.11626] [INSPIRE].

[99] S. Amoroso et al., *Les Houches 2019: Physics at TeV Colliders: Standard Model Working Group Report*, in *11th Les Houches Workshop on Physics at TeV Colliders: PhysTeV Les Houches*, (2020) [arXiv:2003.01700] [INSPIRE].

[100] J. Butterworth et al., *PDF4LHC recommendations for LHC Run II*, *J. Phys. G* **43** (2016) 023001 [arXiv:1510.03865] [INSPIRE].

[101] M. Cacciari, G.P. Salam and G. Soyez, *The anti-k_t jet clustering algorithm*, *JHEP* **04** (2008) 063 [arXiv:0802.1189] [INSPIRE].